CONSTRAINED CENTROIDAL VORONOI TESSELLATIONS FOR SURFACES[*]

QIANG DU[†], MAX D. GUNZBURGER[‡], AND LILI JU[§]

Abstract. Centroidal Voronoi tessellations are useful for subdividing a region in Euclidean space into Voronoi regions whose generators are also the centers of mass, with respect to a prescribed density function, of the regions. Their extensions to general spaces and sets are also available; for example, tessellations of surfaces in a Euclidean space may be considered. In this paper, a precise definition of such constrained centroidal Voronoi tessellations (CCVTs) is given and a number of their properties are derived, including their characterization as minimizers of an "energy." Deterministic and probabilistic algorithms for the construction of CCVTs are presented and some analytical results for one of the algorithms are given. Computational examples are provided which serve to illustrate the high quality of CCVT point sets. Finally, CCVT point sets are applied to polynomial interpolation and numerical integration on the sphere.

Key words. surface tessellations, optimal Voronoi tessellations, surface interpolation, surface quadrature, point sets on surfaces, point sets on the sphere

AMS subject classifications. 65M50, 65N50, 65Y20, 65D05, 65D30

PII. S1064827501391576

1. Introduction. In [1, 2, 3, 4] and [8], a methodology for point placement in regions, i.e., volumes, in $\mathbb{R}^N$ has been developed. The methodology is based on the notion of *centroidal Voronoi tessellations* (CVTs), which is explained in section 1.1. The ensuing methodology produces high-quality point distributions which may themselves be of interest or may be used as a basis for triangulations or Voronoi tessellations of the region. Among the advantages of the CVT methodology is that points may easily be distributed according to a prescribed nonuniform density function and the algorithms which make up the methodology are amenable to parallelization. In addition, CVTs enjoy an optimization characterization so that they themselves turn out to be useful in many applications such as image and data analysis, vector quantization, resource optimization, optimal placement of sensors and actuators for control, cell biology, territorial behavior of animals, numerical partial differential equations, meshless computing, etc.; see, e.g., [1, 2, 3, 5, 10].

The basic definition of the CVT can be generalized to very broad settings that range from abstract spaces to discrete point sets [1]. The purpose of this paper is to study the CVT methodology that was developed in [1, 2, 3, 4] and [8] in the case where the point sets are constrained to lie on surfaces in $\mathbb{R}^N$. There are many instances in which point distributions lying on surfaces or triangulations or more general subdivisions of surfaces are needed. Just to mention a few important examples, there are

[†]Department of Mathematics, Pennsylvania State University, University Park, PA 16802 (qdu@math.psu.edu).

[‡]Department of Mathematics, Iowa State University, Ames IA 50011-2064. Current address: School for Computational Science and Information Technology, Florida State University, Tallahassee FL 322306-4120 (gunzburg@csit.fsu.edu).

[§]Department of Mathematics, Iowa State University, Ames IA 50011-2064. Current address: Institute for Mathematics and its Applications, University of Minnesota, Minneapolis MN 55455-0436 (ju@ima.umn.edu).

geophysical calculations on the surface of the earth, i.e., on nearly a sphere, collocation or nodal points for boundary finite element methods, and the geometric representation of surfaces by panels or other simple objects. Also, many mesh generation methods in three dimensions require that first a surface grid be developed.

The plan of the paper is as follows. After the brief review of CVTs in section 1.1, we develop and analyze, in section 2, the notion of *constrained* CVTs. Then, in section 3, we discuss some deterministic and probabilistic algorithms for the construction of constrained CVTs. In section 4, some computational examples are provided that illustrate the high quality of constrained CVT point sets. Finally, in section 5, we discuss the use of constrained CVT point sets for polynomial interpolation and numerical integration on a sphere.

1.1. Centroidal Voronoi tessellations. We refer to the discussion in [1] for the general definition of CVTs in abstract spaces. We include the case of CVTs in Euclidean spaces here for the sake of completeness. Let $|\cdot|$ denote the Euclidean norm in $\mathbb{R}^N$. Given a bounded open set $\Omega \subset \mathbb{R}^N$ and a set of points $\{\mathbf{z}_i\}_{i=1}^k$ belonging to the closure $\overline{\Omega}$ of Ω, let

$$(1.1) \quad V_i = \{\, \mathbf{x} \in \Omega \;:\; |\mathbf{x} - \mathbf{z}_i| < |\mathbf{x} - \mathbf{z}_j| \quad \text{for } j = 1, \dots, k, \, j \neq i \,\}, \qquad i = 1, \dots, k.$$

Clearly, we have $V_i \cap V_j = \emptyset$ for $i \neq j$ and $\cup_{i=1}^k \overline{V}_i = \overline{\Omega}$. The set $\{V_i\}_{i=1}^k$ is referred to as a *Voronoi tessellation* or *Voronoi diagram* of Ω, the members of the set $\{\mathbf{z}_i\}_{i=1}^k$ are referred to as *generating points* or *generators*, and each V_i is referred to as the *Voronoi region* or *Voronoi cell* corresponding to $\mathbf{z}_i$. It is well known that the Voronoi regions are polyhedra and that they are very useful in a number of applications; see, e.g., [10].

Given a density function $\rho(\mathbf{x}) \geq 0$ defined on $\overline{\Omega}$ and positive and continuous almost everywhere, then, for each Voronoi region V_i, we define its *mass centroid* $\mathbf{z}_i^*$ by

$$(1.2) \qquad \mathbf{z}_i^* = \frac{\displaystyle\int_{V_i} \mathbf{x}\rho(\mathbf{x})\, d\mathbf{x}}{\displaystyle\int_{V_i} \rho(\mathbf{x})\, d\mathbf{x}} \qquad \text{for } i = 1, \dots, k.$$

We call the tessellation defined by (1.1) a CVT if and only if

$$\mathbf{z}_i = \mathbf{z}_i^* \qquad \text{for } i = 1, \dots, k,$$

i.e., each point $\mathbf{z}_i$, which serves as the generator associated with the Voronoi region V_i, is the mass centroid of that region. The existence of centroidal Voronoi tessellations for a given set has been proved, but note that, in general, they are not uniquely defined; see [1].

2. Constrained centroidal Voronoi tessellations. Now consider a compact and continuous surface $\mathbf{S} \subset \mathbb{R}^N$ defined by

$$(2.1) \qquad \mathbf{S} = \{\mathbf{x} \in \mathbb{R}^N \;:\; g_0(\mathbf{x}) = 0 \;\; \text{and} \;\; g_j(\mathbf{x}) \leq 0 \;\text{ for } j = 1, \dots, m\}$$

for some continuous functions g_0 and $\{g_j\}_{j=1}^m$. Similar to (1.1), given a set of points $\{\mathbf{z}_i\}_{i=1}^k \in \mathbf{S}$, one may define their corresponding Voronoi regions on $\mathbf{S}$ by

$$(2.2) \quad V_i = \{\, \mathbf{x} \in \mathbf{S} \;:\; |\mathbf{x} - \mathbf{z}_i| < |\mathbf{x} - \mathbf{z}_j| \quad \text{for } j = 1, \dots, k, \, j \neq i \,\}, \qquad i = 1, \dots, k.$$

For a density function $\rho(\mathbf{x})$ defined on the surface $\mathbf{S}$ and positive almost everywhere, one may encounter a problem with the definition (2.2) when one defines CVTs $\{(\mathbf{z}_i, V_i)\}_{i=1}^k$ of $\mathbf{S}$: the mass centroids $\{\mathbf{z}_i^*\}_{i=1}^k$ of $\{V_i\}_{i=1}^k$ as defined by (1.2) do not in general belong to $\mathbf{S}$. For example, the mass centroid of any region on the surface of a sphere is always located in the interior of the sphere. Therefore, we must first use a generalized definition of a mass centroid on surfaces.

For each Voronoi region V_i, we call $\mathbf{z}_i^c$ the *constrained mass centroid* of V_i on $\mathbf{S}$ if $\mathbf{z}_i^c$ is a solution of the following problem:

$$(2.3) \qquad \min_{\mathbf{z} \in \mathbf{S}} F_i(\mathbf{z}), \qquad \text{where} \qquad F_i(\mathbf{z}) = \int_{V_i} \rho(\mathbf{x}) |\mathbf{x} - \mathbf{z}|^2 \, d\mathbf{x}.$$

The integral over $\{V_i\}$ is understood as standard surface integration on $\mathbf{S}$. Clearly, for each $i = 1, \ldots, k$, $F_i(\cdot)$ is convex. Assume that $\mathbf{z}_1, \mathbf{z}_2 \in \mathbf{S}$; then we have

$$F_i(\mathbf{z}_1) - F_i(\mathbf{z}_2) = \int_{V_i} \rho(\mathbf{x})(|\mathbf{x} - \mathbf{z}_1|^2 - |\mathbf{x} - \mathbf{z}_2|^2) \, d\mathbf{x}.$$

Since $\mathbf{S}$ is compact and $\rho(\cdot)$ is continuous almost everywhere, there exists a constant C such that

$$|F_i(\mathbf{z}_1) - F_i(\mathbf{z}_2)| \leq C|\mathbf{z}_1 - \mathbf{z}_2|.$$

Thus, we know that F_i is continuous and compact, and consequently we obtain the existence of solutions of (2.3); however, the solution may not be unique.

We call the tessellation defined by (2.2) a *constrained centroidal Voronoi tessellation* (CCVT) if and only if the points $\{\mathbf{z}_i\}_{i=1}^k$, which serve as the generators associated with the Voronoi regions $\{V_i\}_{i=1}^k$, are the constrained mass centroids of those regions. Note that although the definition of CCVT conforms with that of CVT for general spaces, it is important to emphasize the main features of the former, namely, the generators are constrained to the surfaces while the distances are still the standard Euclidean distances, not the more general geodesic distances.

For practical applications, it is natural to ask, For a given V_i, how does one find its constrained mass centroid on $\mathbf{S}$, i.e., how does one solve the constrained optimization problem (2.3)? We rewrite (2.3) in the more standard form:

$$(2.4) \qquad \begin{cases} \min_{\mathbf{z} \in \mathbb{R}^N} F_i(\mathbf{z}), \\ g_0(\mathbf{z}) = 0, \\ g_j(\mathbf{z}) \leq 0 \ \text{ for } j = 1, \ldots, m. \end{cases}$$

If $\mathbf{z}_i^c$ is a solution of (2.4), then the Lagrange multiplier rule states that $\mathbf{z}_i^c$ is a stationary point of

$$(2.5) \qquad L_i(\mathbf{z}) = F(\mathbf{z}) - \sum_{j=0}^m \lambda_j g_j(\mathbf{z}) = \int_{V_i} \rho(\mathbf{x}) |\mathbf{x} - \mathbf{z}|^2 \, d\mathbf{x} - \sum_{j=0}^m \lambda_j g_j(\mathbf{z}),$$

where $\lambda_j \in \mathbb{R}$. Under smoothness assumptions on the Lagrange functional, the necessary condition can then be written as

$$(2.6) \qquad \begin{cases} L_{i,z}(\mathbf{z}_i^c) = 0, \\ g_0(\mathbf{z}_i^c) = 0, \\ \lambda_j \geq 0, \ \ \lambda_j g_j(\mathbf{z}_i^c) \leq 0 \ \text{ for } j = 1, \ldots, m. \end{cases}$$

Suppose $\mathbf{z}_i^c$ is not located on the boundary of $\mathbf{S}$, i.e.,

$$g_j(\mathbf{z}_i^c) < 0 \quad \text{for } j = 1, \ldots, m.$$

Then, we know that λ_j must be 0 for all $j = 1, \ldots, m$, and so (2.6) simplifies to

$$(2.7) \qquad 2 \int_{V_i} \rho(\mathbf{x})(\mathbf{x} - \mathbf{z}_i^c) \, d\mathbf{x} - \lambda_0 \nabla_z \big(g_0(\mathbf{z}_i^c)\big) = 0.$$

Furthermore, if $\overline{\lambda} = \frac{\lambda_0}{2}$, we have

$$\int_{V_i} \mathbf{x} \rho(\mathbf{x}) \, d\mathbf{x} = \mathbf{z}_i^c \int_{V_i} \rho(\mathbf{x}) \, d\mathbf{x} + \overline{\lambda} \nabla_z \big(g_0(\mathbf{z}_i^c)\big)$$

or

$$\frac{\displaystyle\int_{V_i} \mathbf{x} \rho(\mathbf{x}) \, d\mathbf{x}}{\displaystyle\int_{V_i} \rho(\mathbf{x}) \, d\mathbf{x}} = \mathbf{z}_i^c + \frac{\overline{\lambda}}{\displaystyle\int_{V_i} \rho(\mathbf{x}) \, d\mathbf{x}} \nabla_z \big(g_0(\mathbf{z}_i^c)\big).$$

Using (1.2), we then obtain

$$(2.8) \qquad \mathbf{z}_i^* - \mathbf{z}_i^c = \frac{\overline{\lambda}}{\displaystyle\int_{V_i} \rho(\mathbf{x}) \, d\mathbf{x}} \nabla_z \big(g_0(\mathbf{z}_i^c)\big)$$

and $g(\mathbf{z}_i^c) = 0$. Thus, we have obtained the following result.

THEOREM 2.1. *For each $i = 1, \ldots, k$, the constrained mass centroids of V_i exist. Furthermore, if $\mathbf{z}_i^c \in \mathbf{S} - \partial\mathbf{S}$ is a constrained centroid of V_i, then $\mathbf{z}_i^* - \mathbf{z}_i^c$ is a vector normal to the surface $\mathbf{S}$ at $\mathbf{z}_i^c$, where $\mathbf{z}_i^*$ is defined by (1.2), i.e., $\mathbf{z}_i^c$ is the projection of $\mathbf{z}_i^*$ onto $\mathbf{S}$ along the normal direction at $\mathbf{z}_i^c$.*

From Theorem 2.1, it is easy to see that the CCVT of a flat surface, i.e., of a surface $\mathbf{S}$ having zero curvature almost everywhere, is reduced to the CVT in the Euclidean space.

There are many available theoretical results for CVTs; see [1]. Similar analyses can be applied to CCVTs. For example, we have the following results.

PROPOSITION 2.2. *Given a compact surface $\mathbf{S} \subset \mathbb{R}^N$ defined by (2.1), a positive integer k, and a positive and measurable density function $\rho(\cdot)$ defined on $\mathbf{S}$, let $\{\mathbf{z}_i\}_{i=1}^k$ denote any set of k points belonging to $\mathbf{S}$ and let $\{V_i\}_{i=1}^k$ denote any tessellation of $\mathbf{S}$ into k regions. Define the* energy functional *or the* distortion value *for $\{(\mathbf{z}_i, V_i)\}_{i=1}^k$ by*

$$(2.9) \qquad \mathcal{F}(\{(\mathbf{z}_i, V_i)\}_{i=1}^k) = \sum_{i=1}^k \int_{\mathbf{x} \in V_i} \rho(\mathbf{x})|\mathbf{x} - \mathbf{z}_i|^2 \, d\mathbf{x}.$$

A necessary condition for $\mathcal{F}$ to be minimized is that the V_i's are the Voronoi regions corresponding to the $\mathbf{z}_i$'s and, simultaneously, the $\mathbf{z}_i$'s are the constrained centroids of the corresponding V_i's, i.e., $\{(\mathbf{z}_i, V_i)\}_{i=1}^k$ is a CCVT of $\mathbf{S}$.

Proof. First examine the first variation of $\mathcal{F}$ with respect to a single point, say $\mathbf{z}_j$. We then have that

$$(2.10) \qquad \mathcal{F}(\mathbf{z}_j + \mathbf{v}) - \mathcal{F}(\mathbf{z}_j) = \int_{\mathbf{x} \in V_j} \rho(\mathbf{x})\big(|\mathbf{x} - \mathbf{z}_j - \mathbf{v}|^2 - |\mathbf{x} - \mathbf{z}_j|^2\big) \, d\mathbf{x},$$

where we have not listed the fixed variables in the argument of $\mathcal{F}$ and where $\mathbf{v}$ is arbitrary such that $\mathbf{z}_j + \mathbf{v} \in \mathbf{S}$. From (2.10), we see that minimizers of $\mathcal{F}$ with respect to $\mathbf{z}_j$ have the same characterization as minimizers of F_j given in (2.3). Thus, the minimizing points $\{\mathbf{z}_j\}_{j=1}^k$ are the constrained centroids of the corresponding regions $\{V_j\}_{j=1}^k$ on $\mathbf{S}$.

Next, for given points $\{\mathbf{z}_i\}_{i=1}^k$ and a tessellation $\{V_i\}_{i=1}^k$ other than the Voronoi tessellation $\{\widetilde{V}_i\}_{i=1}^k$ corresponding to $\{\mathbf{z}_i\}_{i=1}^k$, we may compare

$$(2.11) \qquad \mathcal{F}(\{(\mathbf{z}_i, \widetilde{V}_i)\}_{i=1}^k) = \sum_{i=1}^k \int_{\mathbf{x} \in \widetilde{V}_i} \rho(\mathbf{x}) |\mathbf{x} - \mathbf{z}_i|^2 \, d\mathbf{x}$$

with the value of $\mathcal{F}(\{(\mathbf{z}_i, V_i)\}_{i=1}^k)$ given by (2.9). For a point $\mathbf{x} \in \mathbf{S}$ that belongs to the Voronoi region $\widetilde{V}_j$, we have that

$$(2.12) \qquad \rho(\mathbf{x}) |\mathbf{x} - \mathbf{z}_j|^2 \le \rho(\mathbf{x}) |\mathbf{x} - \mathbf{z}_i|^2 \qquad \text{for } i = 1, \dots, k$$

since possibly $\mathbf{x}$ does not belong to the Voronoi region corresponding to $\mathbf{z}_i$. However, since $\{V_i\}_{i=1}^k$ is *not* a Voronoi tessellation of $\mathbf{S}$ corresponding to $\{\mathbf{z}_i\}_{i=1}^k$, (2.12) must hold with strict inequality over some measure nonzero set of $\mathbf{S}$. Thus,

$$\mathcal{F}(\{(\mathbf{z}_i, \widetilde{V}_i)\}_{i=1}^k) < \mathcal{F}(\{(\mathbf{z}_i, V_i)\}_{i=1}^k)$$

so that $\mathcal{F}$ is minimized when the $\{V_j\}_{j=1}^k$ are chosen to be the Voronoi regions associated with the points $\{\mathbf{z}_j\}_{j=1}^k$. $\quad \square$

Define the functional

$$(2.13) \qquad \mathcal{K}(\{\mathbf{z}_j\}_{j=1}^k) = \sum_{i=1}^k \int_{\mathbf{x} \in \widetilde{V}_i} \rho(\mathbf{x}) |\mathbf{x} - \mathbf{z}_i|^2 \, d\mathbf{x},$$

where $\mathbf{z}_i$'s belong to $\mathbf{S}$ and $\widetilde{V}_i$'s are the corresponding Voronoi regions on $\mathbf{S}$. We call $\mathcal{K}$ the *energy* of $\{\mathbf{z}_j\}_{j=1}^k$ on the surface $\mathbf{S}$. From the above proof, we have the following result.

PROPOSITION 2.3. *Given a surface* $\mathbf{S} \in \mathbb{R}^N$, *a positive integer* k, *and a positive density function* $\rho(\cdot)$ *defined on* $\mathbf{S}$, *then* $\mathcal{F}$ *and* $\mathcal{K}$ *have the same minimizers.*

Let $K = \{\mathbf{Z} = (\mathbf{z}_1, \mathbf{z}_2, \dots, \mathbf{z}_k), \mathbf{z}_j \in \mathbf{S}\}$. Let $A_i = |\widetilde{V}_i|$ denote the area of $\widetilde{V}_i$ and let $\mathbf{A} = (A_1, A_2, \dots, A_k)$. It is obvious that $\mathbf{A}$ is continuous. Furthermore, the following result holds.

THEOREM 2.4. *Let* $\rho(\mathbf{x})$ *be continuous on* Ω. *Then,* $\mathcal{K}$ *is continuous and possesses a global minimum.*

Proof. Let $\mathbf{Z}, \mathbf{Z}' \in K$. Then,

$$(2.14) \qquad |\mathcal{K}(\mathbf{Z}) - \mathcal{K}(\mathbf{Z}')| = \left| \sum_{i=1}^k \left\{ \left(\int_{\mathbf{x} \in \widetilde{V}_i} - \int_{\mathbf{x} \in \widetilde{V}_i'} \right) \rho(\mathbf{x}) |\mathbf{x} - \mathbf{z}_i|^2 \, d\mathbf{x} \right. \right.$$
$$\left. \left. + \int_{\mathbf{x} \in \widetilde{V}_i'} \rho(\mathbf{x}) \left(|\mathbf{x} - \mathbf{z}_i|^2 - |\mathbf{x} - \mathbf{z}_i'|^2 \right) d\mathbf{x} \right\} \right|.$$

Since $\mathbf{S}$ is compact and $\rho(\cdot)$ is continuous, there exists a constant C such that

$$|\mathcal{K}(\mathbf{Z}) - \mathcal{K}(\mathbf{Z}')| \le C \sum_{i=1}^k (|A_i - A_i'| + |\mathbf{z}_i - \mathbf{z}_i'|).$$

Then, the continuity of $\mathcal{K}$ follows from the continuity of $\mathbf{A}$ and the existence of the global minimizer follows from the compactness of $\mathcal{K}$. $\quad\square$

3. Algorithms for determining CCVTs. An arbitrary choice of generating points $\{\mathbf{z}_i\}_{i=1}^k$ on a surface is not, in general, the constrained mass centroid of the corresponding Voronoi regions on that surface. As a result, one is left with the following construction problem: *given a surface* $\mathbf{S} \subset \mathbb{R}^N$, *a positive integer k, and a density function $\rho(\mathbf{x})$ defined for $\mathbf{x} \in \mathbf{S}$, determine a k-point CCVT of $\mathbf{S}$ with respect to the given density function.*

Similar to CVTs of a region, CCVTs of a given surface also are not uniquely defined in general. For example, given a CCVT $\{(\mathbf{z}_i, V_i)\}_{i=1}^k$ on the surface of a sphere with respect to a constant density function, then $\{(\mathbf{z}_i', V_i')\}_{i=1}^k$, a rotation of $\{(\mathbf{z}_i, V_i)\}_{i=1}^k$, is still a CCVT.

3.1. Probabilistic and deterministic methods for determining CCVTs. There are several algorithms known for constructing CCVTs of a given set; see [1, 7, 8, 9]. Here, we consider three methods. The first is *MacQueen's method* [1, 9], a very elegant probabilistic algorithm which divides sampling points into k sets or clusters by taking means of clusters. The second method is a deterministic algorithm that is known in some circles as *Lloyd's method* [1, 7] and which is the obvious iteration between computing Voronoi diagrams and mass centroids. The third method is a probabilistic method suggested in [8] which may be viewed as a generalization of the known MacQueen and Lloyd methods. Using Theorem 2.1, we modify the three methods for the construction of CCVTs.

The modified version of MacQueen's method is given as follows. Throughout, Monte Carlo sampling simply means random sampling according to the given density function.

ALGORITHM 1 (MacQueen's method for CCVTs). *Given a surface* $\mathbf{S}$, *a density function $\rho(\mathbf{x})$ defined for all $\mathbf{x} \in \mathbf{S}$, and a positive integer k,*

0. *choose an initial set of k points $\{\mathbf{z}_i\}_{i=1}^k$ on $\mathbf{S}$, e.g., by using a Monte Carlo method; set $j_i = 1$ for $i = 1, \ldots, k$;*
1. *determine a point $\mathbf{y}$ in $\mathbf{S}$ at random, e.g., by a Monte Carlo method, according to the probability density function $\rho(\mathbf{x})$;*
2. *find a $\mathbf{z}_{i*}$ among $\{\mathbf{z}_i\}_{i=1}^k$ that is the closest to $\mathbf{y}$;*
3. *set*

$$\mathbf{z}_{i*}' \leftarrow \frac{j_{i*}\mathbf{z}_{i*} + \mathbf{y}}{j_{i*} + 1}, \qquad j_{i*} \leftarrow j_{i*} + 1, \qquad and \qquad \mathbf{z}_{i*} = \mathbf{proj}(\mathbf{z}_{i*}');$$

the new $\mathbf{z}_{i*}$, along with the unchanged $\{\mathbf{z}_j\}, j \neq i^*$, form the new set of points $\{\mathbf{z}_i\}_{i=1}^k$;
4. *if the new points meet some convergence criterion, terminate; otherwise, return to step 1.*

In Algorithm 1, $\mathbf{z}_{i*} = \mathbf{proj}(\mathbf{z}_{i*}')$ denotes the following process. If there exists a set $\{\mathbf{z}_{i*}^j\}_{j=1}^r \in \mathbf{S} - \partial\mathbf{S}$, which are projection points of $\mathbf{z}_{i*}'$ onto $\mathbf{S}$ along the normal direction to $\mathbf{S}$ at $\mathbf{z}_{i*}^j$, choose a $\mathbf{z}_{i*}^c$ satisfying $|\mathbf{z}_{i*}^c - \mathbf{z}_{i*}'| = \min_{j=1,\ldots,r} |\mathbf{z}_{i*}^j - \mathbf{z}_{i*}'|$ and then replace $\mathbf{z}_{i*}$ by $\mathbf{z}_{i*}^c$; otherwise, keep $\mathbf{z}_{i*}$ unchanged.

There are two key issues in Algorithm 1 that need to be addressed. The first is how to sample points on a given surface by a Monte Carlo method, i.e., how to do random sampling on a surface according to a given density function. The second concerns the implementation of the projection process. These issues are discussed in section 4.

The almost sure convergence of the energy for the random MacQueen method has been proved in the CVT case; note that in some cases this method fails to converge to a CVT; see [6, 9]. It also has been observed that Macqueen's method converges very slowly and that, in practical computations, the energy of the final set of points is closely correlated to the energy of the corresponding initial set of points; see [8].

The following algorithm is the modification to the CCVT case of Lloyd's method [1, 7].

ALGORITHM 2 (Lloyd's method for CCVTs). *Given a surface* **S**, *a density function* $\rho(\mathbf{x})$ *defined for all* $\mathbf{x} \in \mathbf{S}$, *and a positive integer* k,

0. *select an initial set of* k *points* $\{\mathbf{z}_i\}_{i=1}^k$ *on* **S**, *e.g., by using a Monte Carlo method;*
1. *construct the Voronoi sets* $\{V_i\}_{i=1}^k$ *of* **S** *associated with* $\{\mathbf{z}_i\}_{i=1}^k$;
2. *determine the constrained mass centroids of the Voronoi sets* $\{V_i\}_{i=1}^k$; *these constrained centroids form the new set of points* $\{\mathbf{z}_i\}_{i=1}^k$;
3. *if the new points meet some convergence criterion, terminate; otherwise, return to step* 1.

In Algorithm 2, the determination of constrained mass centroids can be done in two steps: first find the mass centroids and then project them onto the surface **S** using the projection process **proj**. Note that Algorithm 2 requires the explicit construction of Voronoi tessellations of **S** and of the constrained mass centroids of the Voronoi regions.

In the CVT setting, Lloyd's method converges much faster than does MacQueen's method. However, in the CCVT case, one is faced with the difficult task of constructing Voronoi tessellations corresponding to a given set of points on a surface. For a sphere, the STRIPACK package for constructing Voronoi diagrams [11] is available, but similar software is not currently available for general surfaces. This difficulty represents a serious obstacle to the use of the deterministic Lloyd method for determining CCVTs of general surfaces. A variant scheme is to approximate the Voronoi sets using background grids, but the local refinement of background grids for complex density functions is still a substantial problem. Despite this difficulty, Lloyd's method retains considerable theoretical interest.

We next present a modified version, applicable to the CCVT case, of a probabilistic method given in [8] for CVTs. This method can be viewed as a both a probabilistic version of Lloyd's method and as a generalization of the random MacQueen method.

ALGORITHM 3. *Given a surface* **S**, *a density function* $\rho(\mathbf{x})$ *defined for all* $\mathbf{x} \in \mathbf{S}$, *and a positive integer* k,

0. *choose a positive integer* q *and constants* $\{\alpha_i, \beta_i\}_{i=1}^2$ *such that* $\alpha_2 > 0$, $\beta_2 > 0$, $\alpha_1 + \alpha_2 = 1$, *and* $\beta_1 + \beta_2 = 1$; *choose an initial set of* k *points* $\{\mathbf{z}_i\}_{i=1}^k$ *on* **S**, *e.g., by using a Monte Carlo method; set* $j_i = 1$ *for* $i = 1, \ldots, k$;
1. *choose* q *points* $\{\mathbf{y}_r\}_{r=1}^q$ *in* Ω *at random, e.g., by a Monte Carlo method, according to the probability density function* $\rho(\mathbf{x})$;
2. *for* $r = 1, \ldots, q$, *determine a* $\mathbf{z}_{i_r^*}$ *among* $\{\mathbf{z}_i\}_{i=1}^k$ *that is closest to* $\mathbf{y}_r$;
3. *for* $i = 1, \ldots, k$, *gather together in the set* W_i *all sampling points* $\mathbf{y}_r$ *closest to* $\mathbf{z}_i$ *(i.e., in the Voronoi region of* $\mathbf{z}_i$*); if the set* W_i *is empty, do nothing; otherwise, compute the average* $\mathbf{y}_i^*$ *of the set* W_i *and set*

$$\mathbf{z}_i^{*\prime} \leftarrow \frac{(\alpha_1 j_i + \beta_1)\mathbf{z}_i + (\alpha_2 j_i + \beta_2)\mathbf{y}_i^*}{j_i + 1}, \quad j_i \leftarrow j_i + 1, \quad and \quad \mathbf{z}_i^* = \mathbf{proj}(\mathbf{z}_i^{*\prime});$$

the new set of $\{\mathbf{z}_i^*\}$, *along with the unchanged* $\{\mathbf{z}_j\}, j \neq i$, *form the new set of points* $\{\mathbf{z}_i\}_{i=1}^k$;

4. *if the new points meet some convergence criterion, terminate; otherwise, return to step* 1.

Algorithm 3, like MacQueen's method and unlike Lloyd's method, does not require the calculation of Voronoi diagrams on a surface. Note that since two of the α_i's and β_i's are free, Algorithm 3 is actually a two-parameter family of methods. Furthermore, α_1 and β_1 may actually be chosen to be negative, yielding an under-relaxation method. However, for surfaces of closed bodies, e.g., a sphere, one should be careful when using negative values for α_1 and β_1 because then it is possible for the average point $\mathbf{y}_i^*$ to lie outside the body. This, in turn, could complicate the **proj** operation.

Some theoretical and computational analyses of Algorithm 3 (for the CVT case) can be found in [8]. We also note that Algorithm 3 can be parallelized in much the same way it was described in [8] for the standard CVT case.

For the computational examples discussed in section 4, we will use Algorithm 3 with $\alpha_1 = \beta_1 = 0$ so that $\alpha_2 = \beta_2 = 1$. This choice yields a *probabilistic Lloyd's method* in the sense that the integrals that appear in the construction of the centroids are approximated probabilistically by random sampling. In this case, we can expect convergence of the positions of the CCVT points only within sampling error, i.e., the CCVT points can be determined only to within a tolerance related to the error in the evaluation of the centroids by sampling. Thus, it makes no sense to iterate beyond what is required to reduce the movement of the generators to something less than this tolerance. The discussion in [8] concerning the performance of Algorithm 3 for CVTs in the plane and in three dimensions with respect to the various parameters in the algorithm (α_i, β_i, and q) is relevant to the current setting of CVTs on surfaces.

3.2. Some results about Lloyd's method. Let us consider the Lloyd map $\mathbf{Z}_{n+1} = \mathbf{T}(\mathbf{Z}_n)$ on a surface $\mathbf{S}$. From Propositions 2.2 and 2.3, we have

$$(3.1) \quad \mathcal{K}(\mathbf{Z}_{n+1}) = \mathcal{F}(\mathbf{Z}_{n+1}, V(\mathbf{Z}_{n+1})) \leq \mathcal{F}(\mathbf{Z}_{n+1}, V(\mathbf{Z}_n)) \leq \mathcal{F}(\mathbf{Z}_n, V(\mathbf{Z}_n)) = \mathcal{K}(\mathbf{Z}_n),$$

where $V(\mathbf{Z})$ denotes the Voronoi regions of $\mathbf{S}$ associated with $\mathbf{Z}$. From (3.1), we know the Lloyd iteration produces a sequence of points $\{\mathbf{Z}_n\}$ on $\mathbf{S}$ that is bounded and that has monotonically decreasing energy. Applying the above results and a similar proof in [4], we can obtain the following result.

PROPOSITION 3.1. *The set of limit points of a given Lloyd iteration share the same energy $\mathcal{K}$. Consequently, if the fixed point with the same energy is unique, then the Lloyd iteration converges globally.*

It is difficult in general to formulate verifiable conditions on the density function and the geometry of the surface that lead to global convergence. In the following, we will consider a special case.

Let us consider using Lloyd's method of constructing constrained Voronoi tessellations on the unit circle $\mathbf{S} = \{(x, y) \in \mathbb{R}^2 \mid x^2 + y^2 = 1\}$. Let the density function $\rho(\cdot)$ be smooth and strictly positive. For convenience, we represent the unit circle by $\mathbf{S} = \{(\cos(\theta), \sin(\theta)) \mid 0 \leq \theta < 2\pi\}$ and $\rho(\theta) = \rho(\cos(\theta), \sin(\theta))$. In addition, $\rho(\cdot)$ is assumed to satisfy

$$(3.2) \qquad \left(\frac{\rho'(\beta)}{\rho(\beta)} - \frac{\rho'(\alpha)}{\rho(\alpha)}\right) \sin(\alpha - \beta) > 0 \qquad \forall \alpha \neq \beta.$$

Given k points $\mathbf{X} = \{(\cos(\theta_i), \sin(\theta_i)), i = 1, \ldots, k\}$ such that $0 \leq \theta_1 < \theta_2 < \cdots < \theta_k < 2\pi$, clearly, the corresponding Voronoi regions are $V_i = \{(\cos(\theta), \sin(\theta)) :$

$\theta \in \triangle\theta_i\}$, where

$$\triangle\theta_1 = \left(\frac{\theta_k + \theta_1}{2} - \pi, \frac{\theta_1 + \theta_2}{2} \right),$$

(3.3)
$$\triangle\theta_i = \left(\frac{\theta_{i-1} + \theta_i}{2}, \frac{\theta_i + \theta_{i+1}}{2} \right) \quad \text{for } i = 2, \dots, k-1,$$

$$\triangle\theta_k = \left(\frac{\theta_{k-1} + \theta_k}{2}, \frac{\theta_k + \theta_1}{2} + \pi \right).$$

Then, the Lloyd map $\mathbf{T} = (T_1, \dots, T_k)$ can be defined as

(3.4)
$$T_i(\mathbf{X}) = \frac{\mathbf{y}_i}{|\mathbf{y}_i|}, \qquad \text{where} \qquad \mathbf{y}_i = \frac{\displaystyle\int_{V_i} \mathbf{x}\rho(\mathbf{x})\,d\mathbf{x}}{\displaystyle\int_{V_i} \rho(\mathbf{x})\,d\mathbf{x}}.$$

Using (3.3), the $\mathbf{y}_i$'s of (3.4) can be rewritten as

(3.5)
$$\mathbf{y}_i = \left(\frac{\displaystyle\int_{\triangle\theta_i} \rho(\theta)\cos(\theta)\,d\theta}{\displaystyle\int_{\triangle\theta_i} \rho(\theta)\,d\theta} \quad , \quad \frac{\displaystyle\int_{\triangle\theta_i} \rho(\theta)\sin(\theta)\,d\theta}{\displaystyle\int_{\triangle\theta_i} \rho(\theta)\,d\theta} \right).$$

Letting $\Theta = \{\theta_1, \dots, \theta_k\}$, we can redefine the Lloyd map $\mathbf{T} : [0, 2\pi)^k \to [0, 2\pi)^k$ as

(3.6)
$$T_i(\Theta) = \tan^{-1}\left(\frac{\displaystyle\int_{\triangle\theta_i} \rho(\theta)\sin(\theta)\,d\theta}{\displaystyle\int_{\triangle\theta_i} \rho(\theta)\cos(\theta)\,d\theta} \right).$$

Without loss of generality, we assume that $T_i(\Theta) \in [0, \pi/2)$ and $1 < i < k$ since other cases need only a rotation. Let $\theta^- = \frac{\theta_{i-1} + \theta_i}{2}$ and $\theta^+ = \frac{\theta_i + \theta_{i+1}}{2}$; then, we have

(3.7)
$$T_i(\Theta) = \tan^{-1}\left(\frac{\displaystyle\int_{\theta^-}^{\theta^+} \rho(\theta)\sin(\theta)\,d\theta}{\displaystyle\int_{\theta^-}^{\theta^+} \rho(\theta)\cos(\theta)\,d\theta} \right).$$

Let $\phi(\theta) = \rho(\theta)\cos(\theta)$ and $\psi(\theta) = \rho(\theta)\sin(\theta)$. Then, at the fixed point $\Theta = \mathbf{T}(\Theta)$, the Jacobian matrix of the Lloyd map is the tridiagonal matrix

(3.8)
$$\begin{cases} \dfrac{\partial T_i}{\partial \theta_{i-1}} = \dfrac{-\psi(\theta^-) \displaystyle\int_{\theta^-}^{\theta^+} \phi(\theta)\,d\theta + \phi(\theta^-) \displaystyle\int_{\theta^-}^{\theta^+} \psi(\theta)\,d\theta}{2(1 + \tan^2\theta_i)\left(\displaystyle\int_{\theta^-}^{\theta^+} \phi(\theta)\,d\theta \right)^2}, \\[4ex] \dfrac{\partial T_i}{\partial \theta_{i+1}} = \dfrac{\psi(\theta^+) \displaystyle\int_{\theta^-}^{\theta^+} \phi(\theta)\,d\theta - \phi(\theta^+) \displaystyle\int_{\theta^-}^{\theta^+} \psi(\theta)\,d\theta}{2(1 + \tan^2\theta_i)\left(\displaystyle\int_{\theta^-}^{\theta^+} \phi(\theta)\,d\theta \right)^2}, \\[4ex] \dfrac{\partial T_i}{\partial \theta_i} = \dfrac{\partial T_i}{\partial \theta_{i-1}} + \dfrac{\partial T_i}{\partial \theta_{i+1}}. \end{cases}$$

From (3.4) and (3.5), we know that at a fixed point Θ

$$\int_{\theta^-}^{\theta^+} \phi(\theta)\, d\theta = M_i \cos(\theta_i) \quad \text{and} \quad \int_{\theta^-}^{\theta^+} \psi(\theta)\, d\theta = M_i \sin(\theta_i),$$

where $M_i = |\mathbf{y}_i| \int_{\theta^-}^{\theta^+} \rho(\theta)\, d\theta$; then,

(3.9)
$$\begin{cases} \dfrac{\partial T_i}{\partial \theta_{i-1}} = \dfrac{\rho(\theta^-)\sin(\theta_i - \theta^-)}{2M_i(1 + \tan^2 \theta_i)(\cos^2(\theta_i))} = \dfrac{\rho(\theta^-)\sin(\theta_i - \theta^-)}{2M_i}, \\[3mm] \dfrac{\partial T_i}{\partial \theta_{i+1}} = \dfrac{\rho(\theta^+)\sin(\theta^+ - \theta_i)}{2M_i(1 + \tan^2 \theta_i)\cos^2(\theta_i)} = \dfrac{\rho(\theta^+)\sin(\theta^+ - \theta_i)}{2M_i} \end{cases}$$

since $0 < \theta_i - \theta^- = \frac{\theta_i - \theta_{i-1}}{2} < \pi$ and $0 < \theta_+ - \theta_i = \frac{\theta_{i+1} - \theta_i}{2} < \pi$. From (3.9) one easily sees that $\partial \mathbf{T}/\partial \Theta$ at the fixed point is a nonnegative matrix.

Using (3.8) and (3.9), we have

$$M_i\left(1 - \sum_{j=1}^{k} \frac{\partial T_i}{\partial \theta_j}\right) = M_i\left(1 - 2\frac{\partial T_i}{\partial \theta_{i-1}} - 2\frac{\partial T_i}{\partial \theta_{i+1}}\right)$$

$$= M_i - \rho(\theta^-)\sin(\theta_i - \theta^-) - \rho(\theta^+)\sin(\theta^+ - \theta_i)$$

$$= \left(\int_{\theta^-}^{\theta^+} \phi(\theta)\, d\theta\right)^2 + \left(\int_{\theta^-}^{\theta^+} \psi(\theta)\, d\theta\right)^2$$

$$\quad - \left[-\psi(\theta^-)\int_{\theta^-}^{\theta^+} \phi(\theta)\, d\theta + \phi(\theta^-)\int_{\theta^-}^{\theta^+} \psi(\theta)\, d\theta\right]$$

$$\quad - \left[\psi(\theta^+)\int_{\theta^-}^{\theta^+} \phi(\theta)\, d\theta - \phi(\theta^+)\int_{\theta^-}^{\theta^+} \psi(\theta)\, d\theta)\right]$$

$$= \int_{\theta^-}^{\theta^+}\int_{\theta^-}^{\theta^+} \phi(\alpha)\phi(\beta)\, d\alpha d\beta + \int_{\theta^-}^{\theta^+}\int_{\theta^-}^{\theta^+} \psi(\alpha)\psi(\beta)\, d\alpha d\beta$$

$$\quad - \left(\psi(\theta^+) - \psi(\theta^-)\right)\int_{\theta^-}^{\theta^+} \phi(\theta)\, d\theta + \left(\phi(\theta^+) - \phi(\theta^-)\right)\int_{\theta^-}^{\theta^+} \psi(\theta)\, d\theta.$$

Rearranging terms on the right-hand side, we get

$$M_i\left(1 - \sum_{j=1}^{k} \frac{\partial T_i}{\partial \theta_j}\right) = \int_{\theta^-}^{\theta^+}\int_{\theta^-}^{\theta^+} \left[(\phi(\alpha) - \psi'(\alpha))\phi(\beta) + (\psi(\alpha) + \phi'(\alpha))\psi(\beta)\right] d\alpha d\beta$$

$$= \int_{\theta^-}^{\theta^+}\int_{\theta^-}^{\theta^+} \left[-\rho'(\alpha)\rho(\beta)\sin(\alpha)\cos(\beta) + \rho'(\alpha)\rho(\beta)\sin(\beta)\cos(\alpha)\right] d\alpha d\beta$$

$$= \int_{\theta^-}^{\theta^+}\int_{\theta^-}^{\theta^+} \rho'(\alpha)\rho(\beta)\sin(\beta - \alpha)\, d\alpha d\beta$$

$$= \frac{1}{2}\int_{\theta^-}^{\theta^+}\int_{\theta^-}^{\theta^+} (\rho'(\alpha)\rho(\beta) - \rho'(\beta)\rho(\alpha))\sin(\beta - \alpha)\, d\alpha d\beta$$

$$= \frac{1}{2}\int_{\theta^-}^{\theta^+}\int_{\theta^-}^{\theta^+} \rho(\alpha)\rho(\beta)\left(\frac{\rho'(\beta)}{\rho(\beta)} - \frac{\rho'(\alpha)}{\rho(\alpha)}\right)\sin(\beta - \alpha)\, d\alpha d\beta,$$

$$> 0,$$

where the last step follows from (3.2). Thus, by the Gerschgorin theorem, the spectral radius of the Jacobian matrix is less than 1 and we have the local convergence of the Lloyd iteration on the circle.

THEOREM 3.2. *Let* **S** *be the unit circle and assume that* $\rho(\cdot)$ *is a smooth density function that satisfies*

$$\left(\frac{\rho'(\beta)}{\rho(\beta)} - \frac{\rho'(\alpha)}{\rho(\alpha)} \right) \sin(\alpha - \beta) > 0 \qquad \forall \alpha \neq \beta.$$

Then, the Lloyd map **T** *is a local contraction near its fixed points. Consequently, the Lloyd iteration is locally convergent.*

We note that for the case S being a finite one-dimensional interval, a similar result as that in the above theorem holds for logarithmically concave functions, i.e., functions satisfying

$$\left(\frac{\rho'(\beta)}{\rho(\beta)} - \frac{\rho'(\alpha)}{\rho(\alpha)} \right) (\beta - \alpha) < 0 \qquad \forall \alpha, \beta \in S, \alpha \neq \beta.$$

The assumption (3.2) corresponds to a natural generalization of such a condition on the density function in the case S being a circle.

4. Computational examples. Three different surfaces were used to illustrate CCVT point sets. In all examples, Algorithm 3 was used with $\alpha_1 = \beta_1 = 0$ and $\alpha_2 = \beta_2 = 1$. Monte Carlo sampling, i.e., random sampling according to a given density function, on a given surface plays a key role in that method. The main ingredient in our sampling procedure is to use the *rejection method* [12]; the incorporation of this method into our algorithms will be clear. Additionally, we need to implement the projection process **proj** onto a surface.

4.1. CCVTs on the surface of the unit sphere. First, let **S** be the surface of the unit sphere, $\mathbf{S} = \{(x, y, z) \mid x^2 + y^2 + z^2 = 1\}$. The projection process **proj** is quite simple for this surface because of its simple geometry. It is easy to show that the mass centroid of any region of the surface of the unit sphere is always located inside the unit sphere, so the **proj** process can be easily implemented as follows. The projection of a given point (x, y, z) inside the unit sphere (except for the origin, i.e., the center) onto the surface of the sphere is given by

$$\mathbf{proj}(x, y, z) = \frac{1}{r}(x, y, z), \qquad \text{where } r = \sqrt{x^2 + y^2 + z^2}.$$

We use the following procedure to sample points on **S**, the surface of unit sphere, for a given density function $\rho(\cdot)$ defined on **S**.

PROCEDURE 1. *Set* $\widehat{\rho} = \max_{(x,y,z) \in \mathbf{S}} \rho(x, y, z)$;
1. *sample three random numbers* X', Y', *and* Z' *uniformly distributed on* $[0, 1]$; *set* $X = 2X' - 1$, $Y = 2Y' - 1$, *and* $Z = 2Z' - 1$;
2. *set* $R = \sqrt{X^2 + Y^2 + Z^2}$; *if* $0 < R \leq 1$, *then set* $(x, y, z) = \mathbf{proj}(X, Y, Z)$; *otherwise, go to step 1;*
3. *sample another random number* U *uniformly distributed on* $[0, 1]$; *if* $U < \rho(x, y, z)/\widehat{\rho}$, *return* (x, y, z); *otherwise go to step 1.*

Note that step 3 of this procedure is the embodiment of the rejection method mentioned above.

The results of some computationally determined 256-point CCVTs on the unit sphere are given in Figure 4.1. Three different density functions were chosen: a constant density function; $e^{-6.0z^2}$, which has a large variation, i.e., its values range from 1 to e^{-6}, and reaches its maximum on the circle $\{(x, y, z) \mid x^2 + y^2 = 1, z = 0\}$; and $e^{-3.0(1-z)^2}$, which has a large peak at the north pole $(0, 0, 1)$. The Voronoi diagrams were produced using the STRIPACK package [11]. Also, the energies for these tessellations are given in Table 4.1.

Visually, we see from Figure 4.1 that the tessellations of the sphere based on CCVT generators are much more regular than those based on random point sampling. This is also borne out by the results of Table 4.1; the fact that, for the same number of points, the energy of the CCVT tessellations are roughly half those for Monte Carlo–based tessellations is also an indication of the superior regularity of the CCVT tessellations.

4.2. CCVTs on a developable surface. We next choose the developable surface $\mathbf{S} = \{(x, y, z) \mid z = -x^2, |x| \leq \frac{1}{2}, |y| \leq \frac{1}{2}\}$. It is easy to show that the mass centroid of any region of this surface always belongs to the set $Q = \{(x, y, z) \mid |x| < \frac{1}{2}, |y| < \frac{1}{2}, -\frac{1}{4} < z < -x^2\}$. For a given point $(x, y, z) \in Q$, its projection onto $\mathbf{S}$, i.e., $(\widetilde{x}, \widetilde{y}, \widetilde{z}) = \mathbf{proj}(x, y, z)$, is found by solving

$$\frac{2\widetilde{x}(z - \widetilde{z})}{x - \widetilde{x}} = 1, \qquad \widetilde{z} = -\widetilde{x}^2, \qquad \text{and} \qquad \widetilde{y} = y.$$

These may be combined into the cubic equation

$$(4.1) \qquad\qquad \widetilde{x}^3 + \frac{2z + 1}{2}\widetilde{x} - x = 0.$$

Since x always belongs to $(-\frac{1}{2}, \frac{1}{2})$ and z is restricted to $(-\frac{1}{4}, -x^2)$, it is not difficult to verify that (4.1) has only one real solution; thus, $(\widetilde{x}, \widetilde{y}, \widetilde{z})$ is uniquely determined.

A special procedure is given as follows to effect sampling on the developable surface $\mathbf{S}$ for a given density function $\rho(\cdot)$ defined on $\mathbf{S}$.

PROCEDURE 2. *Set $\widehat{\rho} = \max_{(x,y,z) \in \mathbf{S}} \rho(x, y, z)$;*
1. *sample two random numbers X' and Y' uniformly distributed on $[0, 1]$; set $X = X' - \frac{1}{2}$ and $Y = Y' - \frac{1}{2}$;*
2. *set $V = \sqrt{(1 + 4X^2)/2}$ and sample a random number U_1 uniformly distributed in $[0, 1]$; if $U_1 < V$, set $x = X$, $y = Y$, and $z = -x^2$, and go to step 3; otherwise, go to step 1;*
3. *sample another random number U_2 uniformly distributed in $[0, 1]$;*
   if $U_2 < \rho(x, y, z)/\widehat{\rho}$, return (x, y, z); otherwise go to step 1.

Note that the rejection method is invoked in both steps 2 and 3 of this procedure.

The results of some computationally determined 256-point CCVTs on the developable surface are given in Figure 4.2. Two different density functions were chosen: a constant density function and $e^{-20.0x^2}$, which has a large variation, i.e., its values range from 1 to e^{-5} and reaches its maximum on the segment $\{(x, y, z) \mid x = z = 0, y \in [-\frac{1}{2}, \frac{1}{2}]\}$. Since there is currently no software available for determining Voronoi diagrams for a given set of points on such a developable surface, only the positions of the generators are given in Figure 4.2. Visually, we again see from Figure 4.2 that the CCVT points are much more regularly distributed than those obtained by random selection.
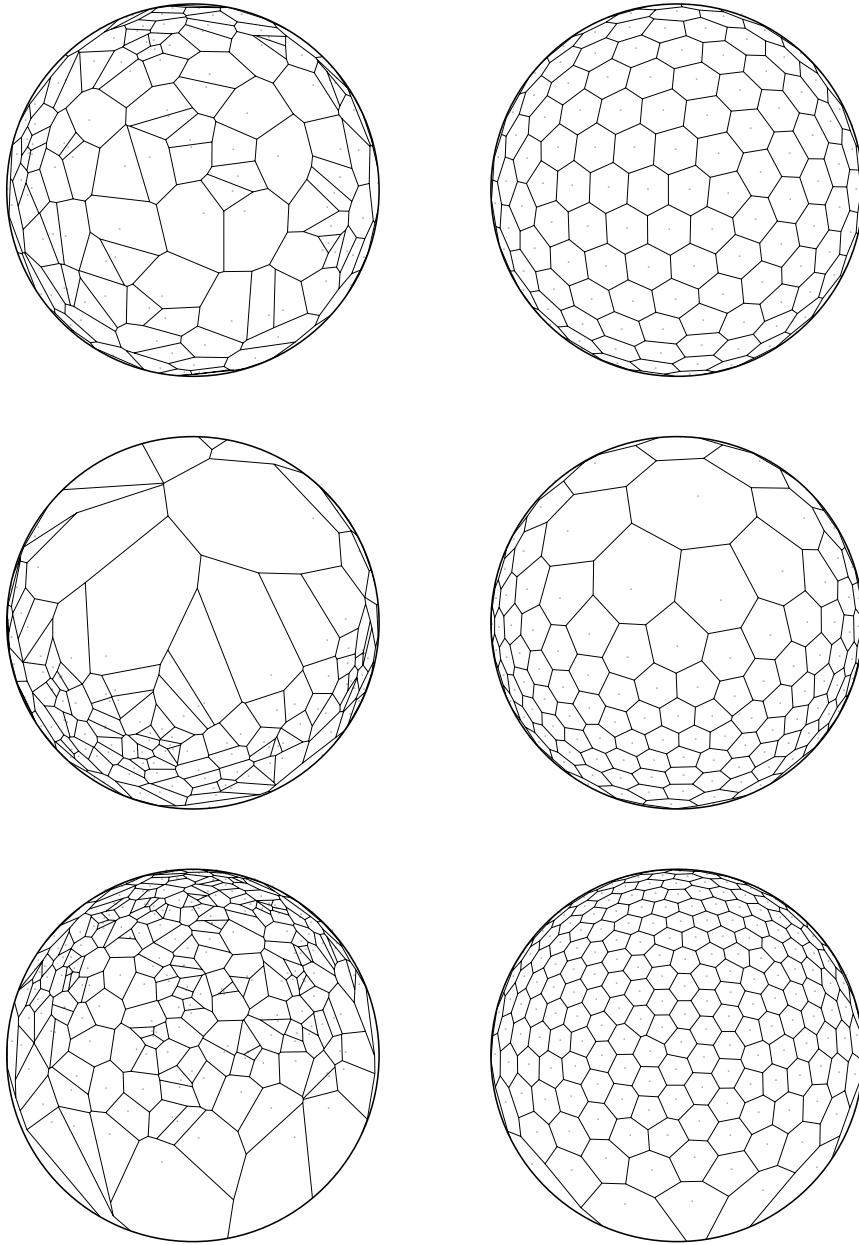
FIG. 4.1. *Voronoi diagrams of* 256 *generators on the surface of unit sphere. Left: Monte Carlo point set; right: constrained CVT point set; top:* $\rho(x, y, z) = 1$*; middle* $\rho(x, y, z) = e^{-6.0z^2}$*; bottom:* $\rho(x, y, z) = e^{-3.0(1-z)^2}$*.*

4.3. CCVTs on the surface of a torus. For the last example, we choose the surface of the torus $\mathbf{S} = \{(x, y, z) \mid (x - \frac{x}{r})^2 + (y - \frac{y}{r})^2 + z^2 = 0.3^2, \ r = \sqrt{x^2 + y^2}\}$. The projection process **proj** for this surface is similar to that for the surface of a sphere but is a little more complicated. It is easy to show that the mass centroid of any region

TABLE 4.1
Energies of 256-point Monte Carlo and CCVTs of a sphere for three density functions.

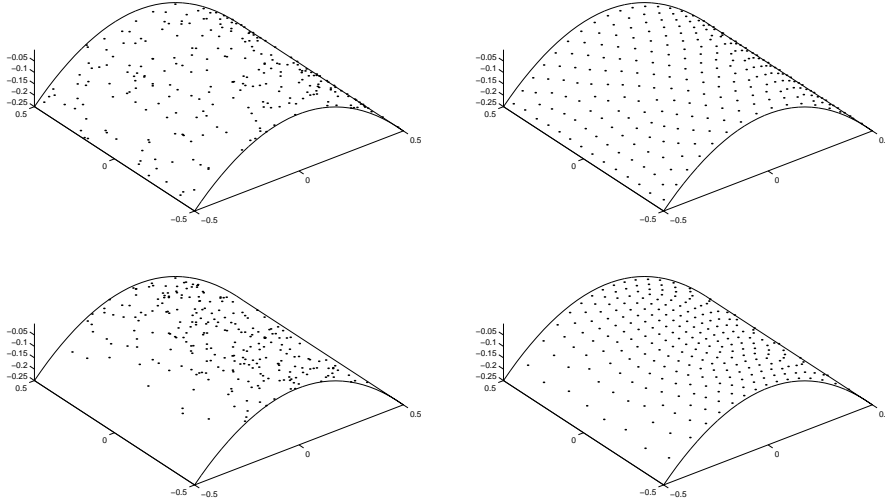| Density function $\rho(x, y, z)$	1	$e^{-6.0z^2}$	$e^{-3.0(1-z)^2}$
Monte Carlo	0.19382	0.05670	0.03081
CCVT	0.09995	0.02533	0.01293

FIG. 4.2. *Voronoi diagrams of* 256 *generators on a developable surface. Left: Monte Carlo point set; right: CCVT point set; top:* $\rho(x, y, z) = 1$; *bottom:* $\rho(x, y, z) = e^{-20.0x^2}$.

of the surface of this torus will always belong to the set $Q = \{(x, y, z) \mid x^2 + y^2 < 1.3^2, |z| < 0.3\}$. Thus, for a given point $(x, y, z) \in Q$ except for the origin $(0,0,0)$, we have

$$\mathbf{proj}(x, y, z) = (\overline{x} + \widehat{x}, \overline{y} + \widehat{y}, \widehat{z}),$$

where

$$\begin{cases} (\overline{x}, \overline{y}) = \dfrac{1}{d}(x, y) \quad \text{and} \quad d = \sqrt{x^2 + y^2}, \\ (\widehat{x}, \widehat{y}, \widehat{z}) = \dfrac{0.3}{d}(x - \overline{x}, y - \overline{y}, z) \quad \text{and} \quad d = \sqrt{(x - \overline{x})^2 + (y - \overline{y})^2 + z^2}. \end{cases}$$

The following procedure is for sampling points on the torus $\mathbf{S}$ for a given density function $\rho(\cdot)$ defined on $\mathbf{S}$.

PROCEDURE 3. *Set* $\widehat{\rho} = \max_{(x,y,z) \in \mathbf{S}} \rho(x, y, z)$;

1. *sample three random numbers* X', Y', *and* Z' *uniformly distributed in* $[0, 1]$; *set* $X = 1.3(2X' - 1)$, $Y = 1.3(2Y' - 1)$, *and* $Z = 0.3(2Z' - 1)$;
2. *set* $R = \sqrt{X^2 + Y^2}$ *and* $V = \sqrt{(X - X/R)^2 + (Y - Y/R)^2 + Z^2}$; *if* $0 < V \leq 0.3$, *then set* $(x, y, z) = \mathbf{proj}(X, Y, Z)$ *and go to step 3; otherwise, go to step 1;*
3. *set* $D = \sqrt{x^2 + y^2 + z^2}$; *sample a random number* W *uniformly distributed in* $[0, 1]$; *if* $W < D/1.3$, *go to step 4.; otherwise go to step 1;*
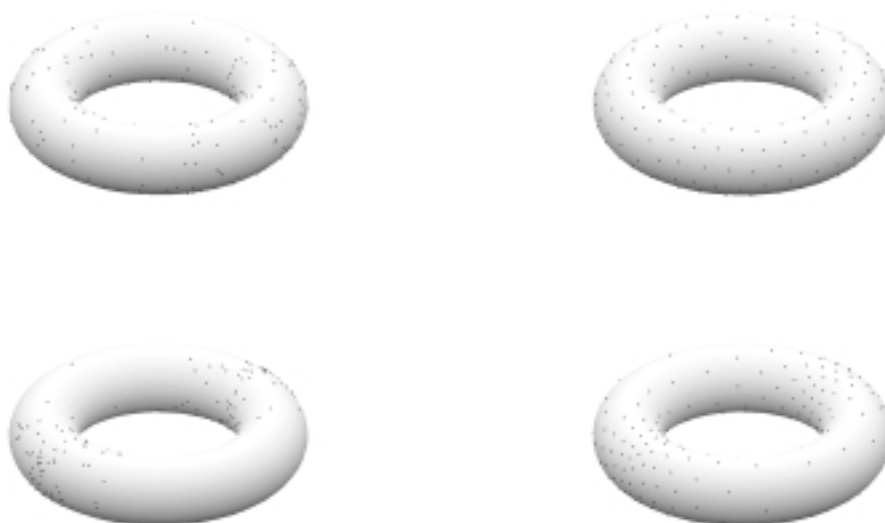
FIG. 4.3. *Voronoi diagrams of* 256 *generators on a torus. Left: Monte Carlo point set; right: CCVT point set; top:* $\rho(x, y, z) = 1$*; bottom:* $\rho(x, y, z) = e^{-5.0|y|}$.

4. *sample a random number U uniformly distributed in* $[0, 1]$*; if* $U < \rho(x, y, z)/\widehat{\rho}$*, return* (x, y, z)*; otherwise go to step* 1.

Again, the rejection method is invoked in steps 2, 3, and 4 of this procedure.

The results of some computationally determined 256-point CCVTs on the torus are given in Figure 4.3. Two different density functions were chosen: a constant density function and $e^{-5.0|y|}$, which has a large variation, i.e., its values range from 1 to $e^{-6.5}$, and reaches its maximum on the two circles $\{(x, y, z) \mid (x - 1)^2 + z^2 = 0.3^2, \, y = 0\}$ and $\{(x, y, z) \mid (x + 1)^2 + z^2 = 0.3^2, \, y = 0\}$. Again, since there is no existing software for determining the Voronoi tessellations on a torus, only the positions of the generators are given in Figure 4.3. Visually, we again see from Figure 4.3 that the CCVT points are much more regularly distributed than those obtained by random selection.

5. CCVTs for interpolation and quadrature on the sphere. We now examine the use of the generators of CVTs of the surface of the sphere for interpolation and quadrature. We will only consider the case of uniformly distributed points, i.e., of a constant density function $\rho(\mathbf{x})$.

The *mesh norm* h of a set of points $\{\mathbf{x}_i\}_{i=1}^{k}$ on the unit sphere S^2 is defined by

$$h = \max_{\mathbf{x} \in S^2} \min_{i=1,\ldots,k} \cos^{-1}(\mathbf{x}^T \mathbf{x}_i).$$

Of course, it is topologically impossible to tessellate the surface of a sphere exactly uniformly. Note, however, that it is clear that a "uniform" tessellation of the surface
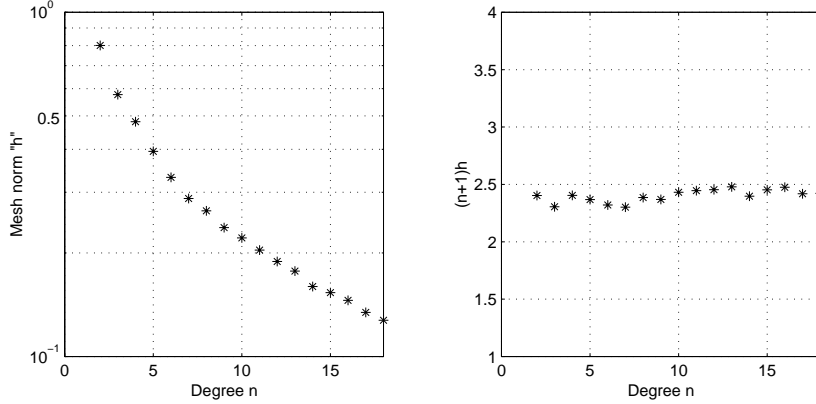
FIG. 5.1. *Mesh norm of CCVT generators vs. degree of the polynomial n; the number of generators $k_n = (n+1)^2$.*

of a sphere into hexagonal-like regions would result in $h\sqrt{k} \approx \sqrt{8\sqrt{3}\pi/9} \approx 2.2$ when k is large. Thus, we can use h as an indicator of the uniformity of point distributions on the sphere. In Figure 5.1, we provide plots of h and $h(n+1)$ vs. n for $k = (n+1)^2$-point CCVTs of the surface of the unit sphere. (We set $k = (n+1)^2$ and refer to n as the *degree* to be consistent with the plot given below for global interpolation on the sphere.) We determine the mesh norm h by sampling 40,000 points $\mathbf{x}$ on the sphere S^2 and then selecting the maximum value of $\min_{i=1,\ldots,k_n} \cos^{-1}(\mathbf{x}^T \mathbf{x}_i)$ over the sampling points. We see from Figure 5.1 that $h(n+1)$ is indeed nearly constant and nearly equal to 2.2 for CCVT point distributions. This implies that CCVT point distributions are very uniform and would be useful for piecewise polynomial interpolation on the sphere and for finite element discretizations of partial differential equations posed on a sphere.

We now consider global polynomial interpolation on the sphere S^2. In [13, 15] good choices of points for this purpose are discussed in detail. Note that if the degree of interpolating polynomial is n, then $k_n = (n+1)^2$ interpolating points $\{\mathbf{x}_i\}_{i=1}^{k_n}$ are needed for global interpolation on the sphere. The "goodness" of a set of interpolation points can be characterized by the uniform norm of the interpolation operator. Following [13, 15], we determine this quantity as follows. Let $\widetilde{G}_n(z) = \frac{n+1}{4\pi}\mathbf{P}_n^{(1,0)}(z)$, where $\mathbf{P}_n^{(a,b)}$ denote the Jacobi polynomials. Define

$$\mathbf{g}(\mathbf{x}) = \left(\widetilde{G}_n(\mathbf{x}^T\mathbf{x}_1), \widetilde{G}_n(\mathbf{x}^T\mathbf{x}_2), \ldots, \widetilde{G}_n(\mathbf{x}^T\mathbf{x}_{k_n})\right)^T$$

and the $k_n \times k_n$ Gram matrix G of the reproducing kernel basis

$$G = \left(\mathbf{g}(\mathbf{x}_1), \mathbf{g}(\mathbf{x}_2), \ldots, \mathbf{g}(\mathbf{x}_{k_n})\right).$$

Then, the uniform norm of the interpolation operator Λ_n is given by

$$\|\Lambda_n\|_{L^\infty} = \max_{\mathbf{x}\in S^2} \|G^{-1}\mathbf{g}(\mathbf{x})\|_{\ell^1}.$$

In Figure 5.2, we provide, for $k_n = (n+1)^2$-point CCVT point distributions, a plot of $\|\Lambda_n\|_{L^\infty}$ vs. n, where n is the degree of the interpolating polynomial. We determine $\|\Lambda_n\|_{L^\infty}$ by sampling 40,000 points $\mathbf{x}$ on the sphere S^2 and then selecting
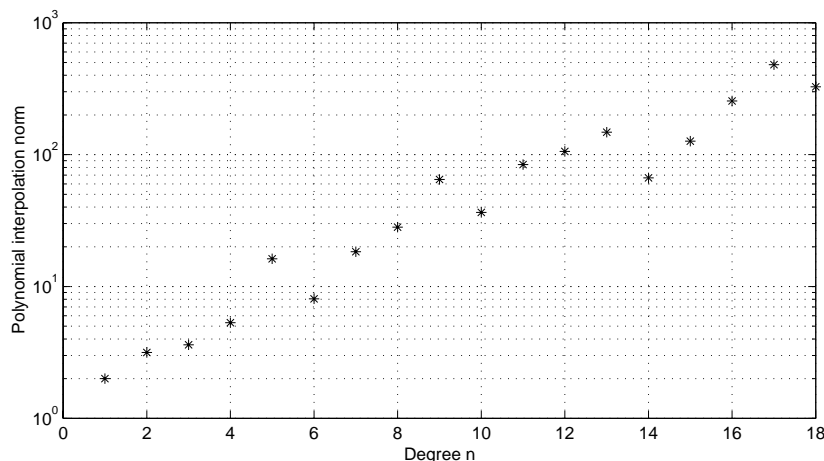
FIG. 5.2. *Global polynomial interpolation norms using CCVT generators vs. degree of the polynomial n; the number of generators $k_n = (n+1)^2$.*

the maximum value of $\|G^{-1}\mathbf{g}(\mathbf{x})\|_{\ell^1}$ over the sampling points. We see from Figure 5.2 that the growth in the log of the norm of the interpolation operator is roughly linear in the degree n of the polynomial; this is the ideal situation.

We next turn to interpolatory quadrature on the surface of the S^2 based on the interpolating polynomial of degree n. If $\{\mathbf{x}_i\}_{i=1}^{k_n}$ is a set of quadrature points, then the quadrature weights are determined by the requirement that

$$\int_{S^2} p(\mathbf{x})\, dx = \sum_{i=1}^{k_n} w_i p(\mathbf{x}_i)$$

for all polynomials p of degree $\leq n$. Following [13, 15], we determine the quadrature weights $\mathbf{w} = (w_1, w_2, \ldots, w_{k_n})$ by solving the linear algebraic system

$$G\mathbf{w} = \mathbf{e},$$

where $\mathbf{e}$ is the vector having all components equal to one. In Figure 5.3, we provide a plot of the maximum and minimum values for the quadrature weights vs. n, the degree of the polynominal. We see that the quadrature weights are all positive and that they are well clustered around the ideal value of unity; in fact, for $n \leq 18$, we have that all the quadrature weights are well within the interval $[0.6, 1.4]$. Again, this is a very good situation for interpolatory quadrature.

In [13, 15] four types of point sets for global interpolation and quadrature on a sphere are compared. One of the point sets is based on minimizing a Coulomb-type potential energy between points; it is dismissed as yielding very large interpolation operator norms and very poor quadrature weights, including some that are negative. CCVT point sets are, in these respects, vastly superior to Coulomb potential point sets. Compared to the other three types of point sets discussed in [13, 15], CCVT point sets are as good as the best of those with respect to quadrature weights; the spread between the maximum and minimum quadrature weights is comparable to that of the best of the point sets discussed in [13, 15]. CCVT points sets are also every bit as good as the best point set of [13, 15] with respect to the mesh norm h.
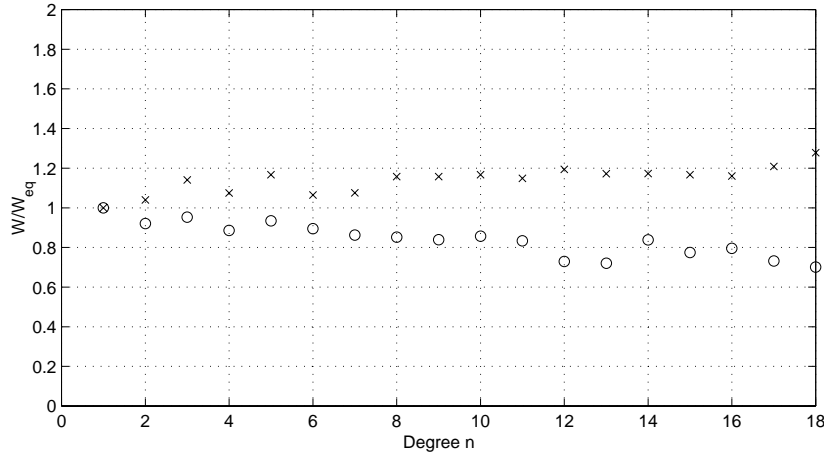
FIG. 5.3. *Maximum and minimum value of the quadrature weights (scaled by $4\pi/k_n$) when the quadrature points are chosen to be CCVT generators vs. degree of the polynomial n; the number of generators is $k_n = (n+1)^2$.*

With respect to the size of the norm of the interpolation operator, CCVT point sets do not perform as well as do the best of the point sets discussed in [13, 15]. However, as shown in Figure 5.2, the growth in this norm for CCVT is acceptable for most practical purposes. Moreover, it is important to note that CCVT point sets may be determined at very much less cost than what is needed for the three good point sets discussed in [13, 15], and the CCVT concept is also applicable to similar problems, i.e., interpolation and quadrature, for more general surfaces.

One important observation is that all three algorithms discussed in section 3 (and indeed all common algorithms for determining CVTs and CCVTs) merely locate *local* minimizers of the energy functional (2.9). This may account for the lack of monotonicity in the plots in Figures 5.1–5.3. Moreover, it is possible that the global minimizers are located so that the performance of CCVT point sets for global interpolation on the sphere would be as good as the best point set discussed in [13, 15]. Algorithms for the determination of CVT and CCVT point sets that are global minimizers of the energy functional (2.9) are currently under study.

Acknowledgment. We thank R. J. Renka for providing his elegant software package STRIPACK for constructing Voronoi diagrams on spheres.

REFERENCES

[1] Q. Du, V. Faber, and M. Gunzburger, *Centroidal Voronoi tessellations: Applications and algorithms*, SIAM Rev., 41 (1999), pp. 637–676.
[2] Q. Du and M. Gunzburger, *Grid generation and optimization based on centroidal Voronoi tessellations*, Appl. Math. Comput., 133 (2002), pp. 591–607.
[3] Q. Du, M. Gunzburger, and L.-L. Ju, *Meshfree, probabilistic determination of point sets and support regions for meshless computing*, Comput. Methods Appl. Mech. Engrg., 191 (2002), pp. 1349–1366.
[4] Q. Du and T. Wong, *On the Lloyd's algorithm for computing CVTs*, Comput. Geom. Anal., submitted.
[5] A. Faulds and B. King, *Sensor location in feedback control of partial differential equation systems*, in Proceedings of the 2000 IEEE International Conference on Control Applications, IEEE Press, Piscataway, NJ, 2000, pp. 536–541.

[6] J. HARTIGAN, *Clustering Algorithms*, John Wiley, New York-London-Sydney, 1975.

[7] S. LLOYD, *Least squares quantization in PCM*, IEEE Trans. Inform. Theory, 28 (1982), pp. 129–137.

[8] L.-L. JU, Q. DU, AND M. GUNZBURGER, *Probabilistic methods for centroidal Voronoi tessellations and their parallel implementations*, J. Parallel. Comput., 28 (2002), pp. 1477–1500.

[9] J. MACQUEEN, *Some methods for classification and analysis of multivariate observations*, in Proceedings of the Fifth Berkeley Symposium on Mathematical Statistics and Probability, Vol. I, L. Le Cam and J. Neyman, eds., University of California, Berkeley, CA, 1967, pp. 281–297.

[10] A. OKABE, B. BOOTS, AND K. SUGIHARA, *Spatial Tessellations: Concepts and Applications of Voronoi Diagrams*, John Wiley, Chichester, UK, 1992.

[11] R. RENKA, *ALGORITHM 772. STRIPACK: Delaunay triangulation and Voronoi diagrams on the surface of a sphere*, ACM Trans. Math. Soft., 23 (1997), pp. 416–434.

[12] S. ROSS, *A First Course in Probability*, 5th ed., Prentice–Hall, Englewood Cliffs, NJ, 1998.

[13] I. SLOAN AND R. WOMERSLEY, *Constructive polynomial approximation on the sphere*, J. Approx. Theory, 103 (2000), pp. 91–118.

[14] R. WOMERSLEY AND I. SLOAN, *How good can polynomial interpolation on the sphere be?*, Adv. Comput. Math., to appear.

[15] R. WOMERSLEY, *Interpolation and Cubature on the Sphere*, http://www.maths.unsw.edu.au/˜rsw/Sphere (15 August 2002).